

High entropy $\text{Sr}((\text{Zr}_{0.94}\text{Y}_{0.06})_{0.2}\text{Sn}_{0.2}\text{Ti}_{0.2}\text{Hf}_{0.2}\text{Mn}_{0.2})\text{O}_{3-x}$ perovskite synthesis by reactive spark plasma sintering

Mattia Biesuz, Shuai Fu, Jian Dong, Anna Jiang, Daoyao Ke, Qiang Xu, Degui Zhu, Mauro Bortolotti, Michael J. Reece, Chunfeng Hu & Salvatore Grasso

To cite this article: Mattia Biesuz, Shuai Fu, Jian Dong, Anna Jiang, Daoyao Ke, Qiang Xu, Degui Zhu, Mauro Bortolotti, Michael J. Reece, Chunfeng Hu & Salvatore Grasso (2019): High entropy $\text{Sr}((\text{Zr}_{0.94}\text{Y}_{0.06})_{0.2}\text{Sn}_{0.2}\text{Ti}_{0.2}\text{Hf}_{0.2}\text{Mn}_{0.2})\text{O}_{3-x}$ perovskite synthesis by reactive spark plasma sintering, Journal of Asian Ceramic Societies, DOI: [10.1080/21870764.2019.1595931](https://doi.org/10.1080/21870764.2019.1595931)

To link to this article: <https://doi.org/10.1080/21870764.2019.1595931>



© 2019 The Author(s). Published by Informa UK Limited, trading as Taylor & Francis Group on behalf of The Korean Ceramic Society and The Ceramic Society of Japan.



Published online: 30 Mar 2019.



Submit your article to this journal [↗](#)




Article views: 147



View Crossmark data [↗](#)

High entropy Sr((Zr_{0.94}Y_{0.06})_{0.2}Sn_{0.2}Ti_{0.2}Hf_{0.2}Mn_{0.2})O_{3-x} perovskite synthesis by reactive spark plasma sintering

Mattia Biesuz ^{a,b}, Shuai Fu^a, Jian Dong^a, Anna Jiang^a, Daoyao Ke^a, Qiang Xu^a, Degui Zhu^a, Mauro Bortolotti ^c, Michael J. Reece^b, Chunfeng Hu^a and Salvatore Grasso^a

^aKey Laboratory of Advanced technologies of Materials, Ministry of Education, School of Materials Science and Engineering, Southwest Jiaotong University, Chengdu, China; ^bSchool of Engineering and Material Science, Queen Mary University of London, London, UK; ^cDepartment of Industrial Engineering, University of Trento, Trento, Italy

ABSTRACT

A rising interest in entropy-stabilized oxides in recent years has been driven by their attractive functional properties. Their synthesis usually requires prolonged exposure at high temperature to promote solid-state diffusion without the application of pressure. In this work, we report the synthesis of a high entropy perovskite, Sr((Zr_{0.94}Y_{0.06})_{0.2}Sn_{0.2}Ti_{0.2}Hf_{0.2}Mn_{0.2})O_{3-x} in a relatively short time (minutes instead of hours) using a spark plasma sintering (SPS) furnace. Comparative analysis showed that conventional pressureless sintering at 1500°C for 2 h results in porous materials with large thermodynamically stable pores (tens of μm), while SPS processing produces dense materials in a single step by reactive sintering at 1475°C in 9 min. SPS is therefore an attractive route for the production, synthesis and sintering of dense high-entropy oxides.

ARTICLE HISTORY

Received 16 January 2019
Accepted 25 February 2019

KEYWORDS

High entropy; entropy-stabilized oxides; perovskite; SPS; reactive SPS

1. Introduction

Although high entropy alloys have been known for several years in the field of metallurgy [1–3], high entropy ceramics, in particular oxides, were synthesized only as recently as 2015. Starting with pioneering work by Rost et al. [4], this a class of novel ceramics has attracted growing attention in the scientific community. Configurational entropic stabilization opens up a broad field of study aimed at facilitating the production of materials in completely novel compositional spaces. The possibility of introducing “*n*” different elemental components into an oxide structure allows ultra-fine tuning of material properties by changing their composition in a space with “*n*–1” degrees of freedom. The same concept has also been applied to other ceramics, such as carbides [5–7] and other covalent compounds [8,9].

In the past few years, research in the field of entropy-stabilized oxides (E-SOs) has diversified into four main topics. The first is aimed at exploring their potential in terms of functional properties [8]; these include their dielectric constant and loss tangent [10], thermal conductivity [11,12], lithium ion conductivity [13] and energy storage [14]. Other research has focused on reaching a deeper understanding of the structural and thermodynamic properties of these materials [15–19]. Recent research has investigated the synthesis of new E-SOs and sought to identify a correlation between their crystal

structures and compositions [11,20–24]. Finally, novel synthesis routes suitable for E-SOs have been investigated [25–29].

E-SOs are generally produced by solid-state synthesis, where long (several hours), high-temperature thermal treatment allows the formation of a single phase material starting from a mixture containing different oxide powders. However, this approach involves some weaknesses, including the following: (i) thermal treatments usually involve long dwell times at high temperature (in the order of hours), which might affect the final composition because of the preferential volatilization of one of the phases; (ii) the pellets obtained after the thermal treatment are often porous [13,16], possibly requiring further pulverization and sintering treatment; and (iii) high-temperature phase transformation may be competitive with sintering, thus contributing to the formation of internal stresses and physical defects.

Conducted with the aim of reducing the synthesis time and producing dense, defect-free components in a single step, this study investigated the application of spark plasma sintering (SPS) to reactive sinter an E-SO. This report focuses on the high entropy Sr((Zr_{0.94}Y_{0.06})_{0.2}Sn_{0.2}Ti_{0.2}Hf_{0.2}Mn_{0.2})O_{3-x} perovskite, whose conventional synthesis had already been investigated [22] but whose sintering behavior has not been previously analyzed. Both conventional and SPSed samples were produced to elucidate the SPS effect on synthesis and sintering of Sr((Zr_{0.94}Y_{0.06})_{0.2}Sn_{0.2}Ti_{0.2}Hf_{0.2}Mn_{0.2})O_{3-x}.

CONTACT Chunfeng Hu  chfhu@live.cn; Salvatore Grasso  chfhu@live.cn  School of Materials Science and Engineering, Southwest Jiaotong University, Chengdu 610031, China

© 2019 The Author(s). Published by Informa UK Limited, trading as Taylor & Francis Group on behalf of The Korean Ceramic Society and The Ceramic Society of Japan. This is an Open Access article distributed under the terms of the Creative Commons Attribution License (<http://creativecommons.org/licenses/by/4.0/>), which permits unrestricted use, distribution, and reproduction in any medium, provided the original work is properly cited.

2. Experimental procedures

The raw materials used were as follows: MnO₂ (Shanghai Yunfu Nanotechnology Co., China, manganese dioxide 99.9%, 1 μm), SnO₂ (244,651 Sigma Aldrich, 99.9, <50 μm), 3YSZ (Tosoh, TZ-3YS-E, Japan, SSA = 7 m²/g), SrO (Shanghai Yunfu Nanotechnology Co., China, 99.9%, 1 μm), TiO₂ (Sigma Aldrich, Anatase, 99.8%, <5μm) and HfO₂ (ABCR Gute Chemie, Gemany, *d*₉₀ = 1). All of the components were mixed in the appropriate amount to obtain 20 g of the target composition Sr((Zr_{0.94}Y_{0.06})_{0.2}Sn_{0.2}Ti_{0.2}Hf_{0.2}Mn_{0.2})O_{3-x}. The powder mixture was ball-milled in a polyethylene jar for 24 h using 10 g alumina balls. Since the process was low-energy rotary ball-milling, no significant modification of the granulometric distribution was expected.

The powder used for conventional sintering was mixed with 2.5 wt% of binder (QPAC® 40) dissolved in acetone. After drying, the powders were shaped by uniaxial pressing at 250 MPa into bar-like specimens with cross-sections of 3 × 20 mm². The weight of each sample was about 0.8 g. Conventional sintering was carried out by heating the specimens to 1400°C and 1500°C for 2 h (heating rate 2°C/min up to 400°C and 10°C/min from 400°C to the final sintering temperature). About 6 g of loose powder was used to produce SPS samples of 20 mm diameter. The consolidation was carried out in a Chenhua 10–20 SPS furnace (China). The thermal and pressure cycles are reported in Table 1. The temperature was measured using a pyrometer with a 1 cm thick wall pointed at the die surface (hollow cylinder). The SPS sintering temperatures were set at 1450°C and 1375°C, which are slightly lower than those used for conventional sintering. Application of external pressure during SPS allowed a reduction of the consolidation temperature.

The density of the sintered samples was measured by the Archimedes' method using an analytical scale with a sensitivity of 10⁻⁴ g. Phase analysis was carried out by XRD (Bruker D8 Advance A25X (XRD, Bruker AXS GMBH, Cu Kα radiation, 2θ = 20–80°). SEM micrographs were taken of the fracture surfaces of the sintered ceramics using an FEI Inspect F50 (secondary electrons imaging, 10 kV electron source).

3. Results and discussion

Figure 1 shows the SPS piston displacement during the thermal cycle for a sample treated up to 1450°C. One can observe the presence of four main shrinkage events indicated by Greek letters (Figure 1(b)). The first event, α, which took place at room temperature and corresponded to the application of pressure, was due to compacting of the powder. The second, β, took place just before the sample temperature reached 600°C (note that temperatures below 600°C cannot be measured with an SPS pyrometer). This phenomenon appears likely to be related to the melting of MnO₂, which has a melting temperature of 535°C. The formation of the liquid phase causes particle rearrangement and volumetric shrinkage corresponding to the early stage of liquid phase sintering [30,31]. The molten MnO₂ did not leak out of the die but, rather, filled the porosity. The third event, γ, observed between 1000°C and 1250°C, appears to have been related to the densification of the ceramic. Here, a plateau was reached that lasted up to 1450°C, where the high temperature combined with an increase in external pressure produced further shrinkage and densification. Note that some shrinkage also took place during cooling, due to the thermal contraction of the SPS graphite tooling.

Phase analyses of the various samples are presented in Figure 2. Most of the materials are present as the main target high entropy perovskite phase (peak indexing from crystallographic data in [26]). Undesirable secondary phases (indicated by arrows) can still be detected, in particular in the sample treated by SPS at 1375°C for 9 min; the presence of secondary phases was negligible for the sample treated by SPS at 1450°C. SPS therefore appears to be an effective synthesis route for production of these materials, allowing effective reactions between the different components in relatively short times. In fact, in the case of the SPS-treated samples, the reaction produced an almost completely perovskite phase in less than 10 min, while conventional synthesis routes usually require hours [22]. This is likely due to the fact that the application of external pressure results in more rapid sintering (by increasing the driving force

Table 1. Thermal and pressure schedule used for SPS cycles.

Stage	SPS 1450°C, 9 min		SPS 1375°C, 9 min	
1	From 25°C to 600°C, heating rate not controlled (35% of the maximum power output) From 600 to 700°C, 10°C/min	From 15 to 30 MPa, 1.36 MPa/min	From 25°C to 600°C, heating rate not controlled (35% of the maximum power output) From 600 to 700°C, 10°C/min	From 15 to 30 MPa, 1.36 MPa/min
2	From 700°C to 1450°C, 70°C/min	30 MPa constant	From 700°C to 1375°C, 70°C/min	30 MPa constant
3	1450°C for 9 min	From 30 to 50 MPa, 2.2 MPa/min	1375°C for 9 min	From 30 to 50 MPa, 2.2 MPa/min
4	From 1450°C to 700°C, -90°C/min	From 50 to 30 MPa, -2.40 MPa/min	From 1375°C to 700°C, -90°C/min	From 50 to 30 MPa, -2.86 MPa/min
5	Free cooling	0 MPa	Free cooling	0 MPa

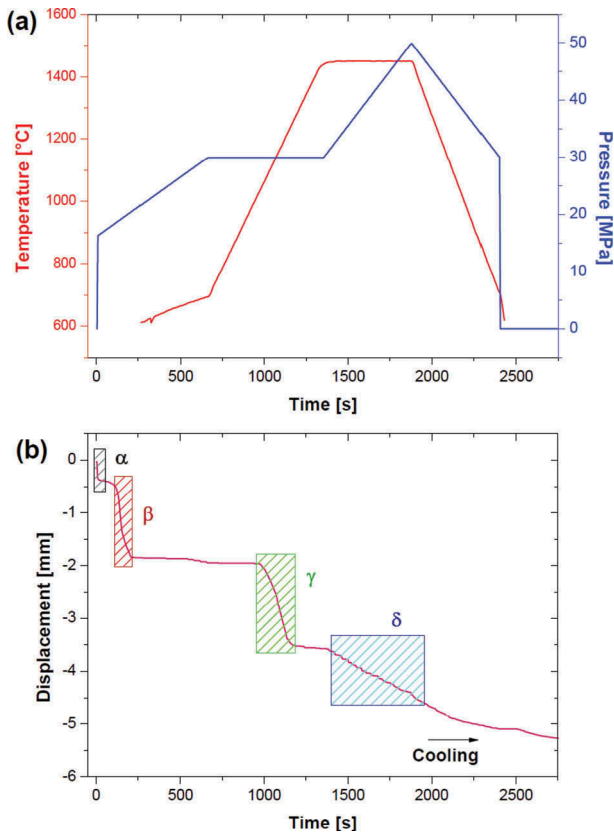


Figure 1. (a) Temperature and pressure and (b) linear shrinkage recorded during SPS cycles of the powder mixture (temperatures below 600°C are not reported because undetectable by SPS pyrometer).

for densification), and the more rapid neck growth enlarges the path through which inter-diffusion takes place. It is therefore expected to accelerate the solid-state reactions leading to formation of the high entropy perovskite structure. However, additional field-induced effects or phenomena associated with the strong reduction conditions inside the SPS apparatus cannot be excluded a priori.

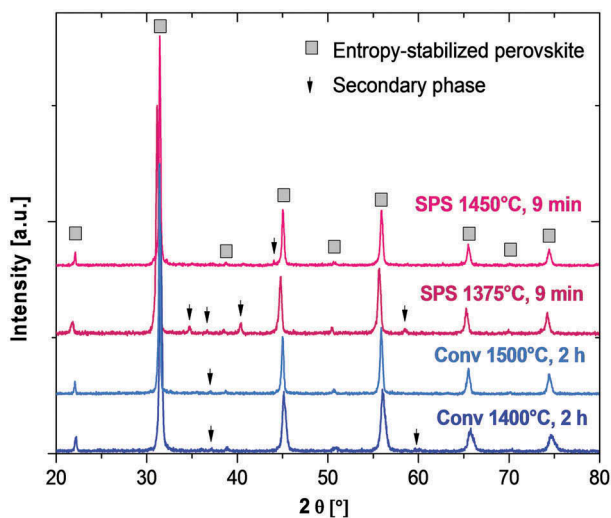


Figure 2. XRD patterns of the materials produced by SPS and conventional sintering.

The results of density and porosity measurements of the sintered samples are reported in Table 2. It can be observed that both the samples treated by SPS achieved an extremely high level of densification with negligible presence of open porosity. The final density remained substantially unchanged whether the treatment was carried out at 1450°C or 1375°C, suggesting that the densification process was almost completed at 1375°C. This indicates that the densification during SPS was concluded before conversion to the high entropy perovskite was completed; peaks associated with secondary phases were still clearly visible in the sample processed by SPS at 1375°C (Figure 2). Under these conditions E-SO formation must have taken place only through solid state diffusion, other such phenomena as evaporation-condensation or surface diffusion being excluded. The theoretical density of the E-SO, as estimated from the XRD cell parameter measured on the sample processed by SPS at 1450°C ($a = 4.032984 \text{ \AA}$), is in the range 5.91–5.92 g/cm³, depending on the charge compensation mechanism for trivalent Y doping. This theoretical density is closely similar to that measured after SPS at 1450°C. This calculation cannot be replicated for specimens undergoing SPS at lower temperatures because of the presence of secondary phases. On this basis, an SPS cycle at 1450°C represents the optimal sintering route, allowing: (i) formation of an almost pure single-phase material; and (ii) completion of the densification process with few residual pores. Lower sintering temperatures, as in the case of the sample processed by SPS at 1375°C, did not allow a complete reaction between the powders, whereas sintering at a higher temperature is less environmentally efficient and promotes grain coarsening.

The bulk density of the conventionally sintered sample treated for 2 h at 1500°C is about 84% of the sample processed by SPS at 1450°C for 9 min. An even lower density was achieved in the case of the sample conventionally treated at 1400°C, where the bulk density was only ~60%. The decrease in apparent density when increasing the sintering temperature from 1400 to 1500°C is consistent with a transition from open to closed porosity, which is in agreement

Table 2. Bulk and apparent density and open porosity (P_{open}) of samples processed at different temperatures by SPS and conventional sintering.

	Bulk density [g/cm ³]	P_{open} %	Apparent density [g/cm ³]
SPS 1450°C, 9 min	5.90	0.04	5.91
SPS 1375°C, 9 min	5.89	0.04	5.90
Conv 1500°C, 2 h	4.97	9.00	5.47
Conv 1400°C, 2 h	3.58	37.27	5.71

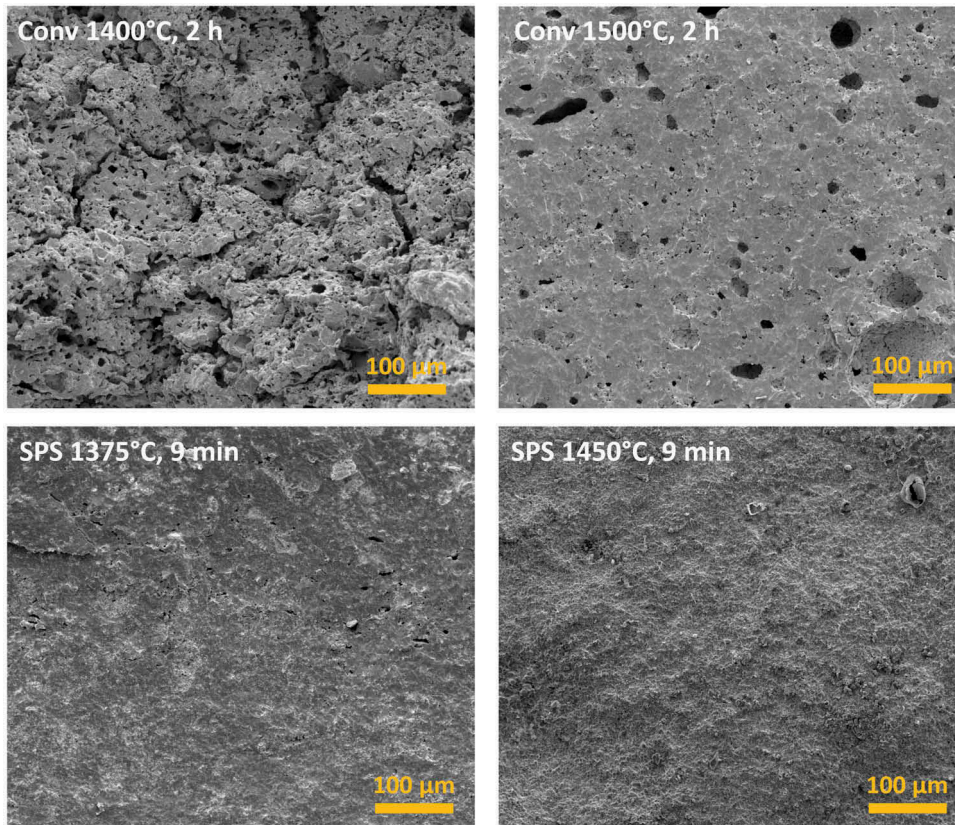


Figure 3. Low-magnification SEM micrographs of fracture surfaces of sintered samples.

with the Significant decrease in the former as reported in Table 2.

SEM investigation of the sintered samples' microstructures confirmed the results of the density measurements. The low-magnification micrographs in Figure 3 indicate that conventional sintering produces porous microstructures with relatively large pores (on the order of a few tens of μm). The porosity appears to be interconnected in the sample treated at 1400°C , whereas it becomes more closed in that sintered at 1500°C . The origin of this large porosity is not completely clear. It seems unlikely that it originated during pressing as a result of poor-plastic deformation of the powder granules; in fact, no granules can be identified in the sintered microstructures. Its origin might be connected to the formation of the MnO_2 -based liquid phase, as a result of inhomogeneous wetting of the solid particles or of the dissolution of the liquid phase within the solid during the reactive sintering process. Indeed, it is well-known that if a liquid phases dissolves inside a solid during sintering it causes the formation of abundant porosity (a phenomenon also known as “swelling”) [30,31]

The higher magnification micrographs (Figure 4) indicate that in conventional sintering the material between these large pores is substantially dense in the cases of both the 1400 and 1500°C treatments. A significant coarsening phenomenon can also be observed in the sample treated at 1500°C , with the

grain size approaching about $5\ \mu\text{m}$. The grain morphology at the pore surface assumes a convex shape as a result of the large pore-to-grain size ratio. The curvature-induced stresses on the material surrounding the surface are therefore compressive, leading to thermodynamic stabilization of the pores themselves [30]. This kind of porosity cannot therefore be eliminated by increasing either the sintering time or temperature, until the grain coarsening phenomenon becomes sufficient to reduce the number of grains surrounding a single pore significantly. In fact, the pore stability/instability conditions can be easily described in light of some definitions reported by Rahaman [30] using simple geometric and algebraic manipulations. In particular, we can state that pores become unstable and shrink during pressure-less conventional sintering only when:

$$m < \frac{360}{180 - \varphi} \quad (1)$$

where m is the number of grains surrounding the pores and φ is the dihedral angle in degrees.

Conversely, micrographs of the materials produced by SPS show a long-range homogeneous microstructure with just a few residual pores in the case of the sample treated at 1375°C . Such densification levels can be achieved because the application of an external pressure of just several MPa overcomes the thermodynamic stabilization of the large pores

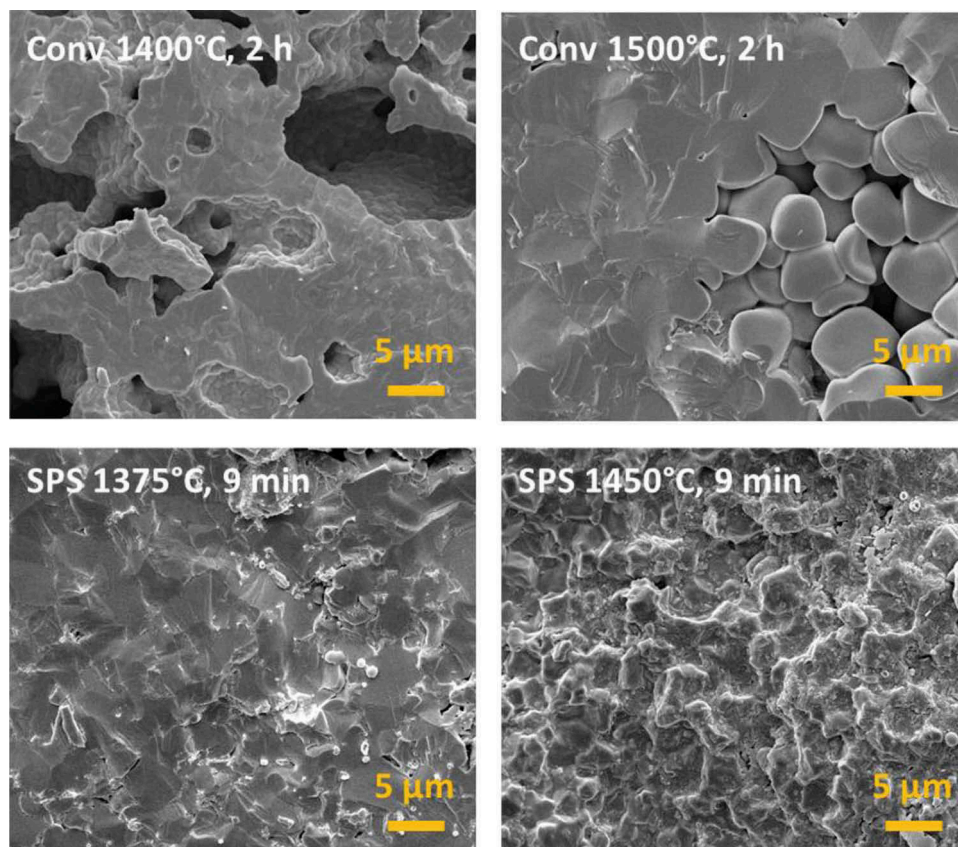


Figure 4. High-magnification SEM micrographs of fracture surfaces of sintered samples.

observed during conventional sintering. A fracture mechanics transition from trans- to inter-granular is also observed when increasing the SPS processing temperature (Figure 4): the sample processed by SPS at 1375°C presents a “flat” fracture surface with cleavages passing through the grains, whereas in the sample processed by SPS at 1450°C the crack is propagated between the grains. The origin of the fracture mechanism transition in SPS processed samples is still not clear. This seems to be related not just to the processing temperature, which causes a more complete development of the E-SO phase or might produce grain boundary segregation; in fact, trans-granular fracture appears to be dominant in both the conventionally sintered samples, including the single-phase sample processed at 1500°C for 2 h. We can tentatively suggest that this might be an effect of the strong reduction conditions in SPS (low oxygen partial pressure and the presence of graphitic carbon and electric currents), which promote modification of the point defect chemistry (and their grain boundary segregation), especially at high temperatures. Further investigation is needed to clarify this issue.

4. Conclusions

SPS is a valuable technology for the production of a high entropy perovskite in the $\text{Sr}((\text{Zr}_{0.94}\text{Y}_{0.06})_{0.2}\text{Sn}_{0.2}\text{Ti}_{0.2}\text{Hf}_{0.2}\text{Mn}_{0.2})\text{O}_{3-x}$ system. It allows

a substantial reduction in the reaction time needed for conversion into a high entropy structure, and remarkably improves the densification process. In particular, SPS allows reactive sintering in a single step to produce dense components, which cannot be attained by conventional sintering.

Acknowledgments

This work is supported by Thousand Talents Program of China and Sichuan Province, the Open Project of State Key Laboratory Cultivation Base for Nonmetal Composites and Functional Materials (17kffk01), Outstanding Young Scientific and Technical Talents in Sichuan Province (2019JDJQ0009), and the Natural Sciences Foundation of China (No. 51741208).

Disclosure statement

No potential conflict of interest was reported by the authors.

ORCID

Mattia Biesuz  <http://orcid.org/0000-0002-4338-4177>
Mauro Bortolotti  <http://orcid.org/0000-0002-7213-6316>

References

- [1] Wong SK, Shun TT, Chang CH, et al. Microstructures and properties of $\text{Al}_{0.3}\text{CoCrFeNiMnx}$ high-entropy alloys. *Prog Mater Sci.* 2014;61:1–93.

- [2] Yeh JW, Chen SK, Lin SJ, et al. Nanostructured high-entropy alloys with multiple principal elements: novel alloy design concepts and outcomes. *Adv Eng Mater.* 2004;6:299–303.
- [3] Cantor B, Chang ITH, Knight P, et al. Microstructural development in equiatomic multicomponent alloys. *Mater Sci Eng A.* 2004;375–377:213–218.
- [4] Rost CM, Sacht E, Borman T, et al. Entropy-stabilized oxides. *Nat Commun.* 2015;6:8485.
- [5] Castle E, Csanádi T, Grasso S, et al. Processing and properties of high-entropy ultra-high temperature carbides. *Sci Rep.* 2018;8:8609.
- [6] Dusza J, Švec P, Girman V, et al. Microstructure of (Hf-Ta-Zr-Nb)C high-entropy carbide at micro and nano/atomic level. *J Eur Ceram Soc.* 2018;38:4303–4307.
- [7] Xueliang Y, Constantin L, Lu Y, et al. (Hf_{0.2}Zr_{0.2}Ta_{0.2}Nb_{0.2}Ti_{0.2})C high-entropy ceramics with low thermal conductivity. *J Am Ceram Soc.* 2018. IN PRESS. DOI:10.1111/jace.15779
- [8] Gao MC, Miracle DB, Maurice D, et al. High-entropy functional materials. *J Mater Res.* 2018;1–18. DOI:10.1557/jmr.2018.323
- [9] Gild J, Zhang Y, Harrington T, et al. High-entropy metal diborides: a new class of high-entropy materials and a new type of ultrahigh temperature ceramics. *Sci Rep.* 2016;6:37946.
- [10] Bérardan D, Franger S, Dragoe D, et al. Colossal dielectric constant in high entropy oxides. *Phys Status Solidi - Rapid Res Lett.* 2019;10:328–333.
- [11] Chen K, Pei X, Tang L, et al. A five-component entropy-stabilized fluorite oxide. *J Eur Ceram Soc.* 2018;38:4161–4164.
- [12] Lim M, Rak Z, Braun JL, et al. Influence of mass and charge disorder on the phonon thermal conductivity of entropy stabilized oxides determined by molecular dynamics simulations. *J Appl Phys.* 2019;125:55105.
- [13] Bérardan D, Franger S, Meena AK, et al. Room temperature lithium superionic conductivity in high entropy oxides. *J Mater Chem A.* 2016;4:9536–9541.
- [14] Sarkar A, Velasco L, Wang D, et al. High entropy oxides for reversible energy storage. *Nat Commun.* 2018;9:3400.
- [15] Anand G, Wynn AP, Handley CM, et al. Phase stability and distortion in high-entropy oxides. *Acta Mater.* 2018;146:119–125.
- [16] Berardan D, Meena AK, Franger S, et al. Controlled Jahn-Teller distortion in (MgCoNiCuZn)O-based high entropy oxides. *J Alloys Compd.* 2017;704:693–700.
- [17] Usharani NJ, Kumar RN, Bhattacharya SS Phase evolution during synthesis of nanocrystalline multicomponent (Co,Cu,Mg,Ni,Zn)O Metal Oxides with Varying ZnO content. *Proc. 2nd World Congr; 2017 Apr 4–6; Barcelona, Spain. Recent Adv. Nanotechnol.* p. 143.
- [18] Rak Z, Rost CM, Lim M, et al. Charge compensation and electrostatic transferability in three entropy-stabilized oxides: results from density functional theory calculations. *J Appl Phys.* 2016;120:95105.
- [19] Rost CM, Rak Z, Brenner DW, et al. Local structure of the Mg_xNi_xCo_xCu_xZn_xO(_x=0.2) entropy-stabilized oxide: an EXAFS study. *J Am Ceram Soc.* 2017;100:2732–2738.
- [20] Djenadic R, Sarkar A, Clemens O, et al. Multicomponent equiatomic rare earth oxides. *Mater Res Lett.* 2017;5:102–109.
- [21] Dąbrowa J, Stygar M, Mikuła A, et al. Synthesis and microstructure of the (Co,Cr,Fe,Mn,Ni)₃O₄ high entropy oxide characterized by spinel structure. *Mater Lett.* 2018;2016:32–36.
- [22] Jiang S, Hu T, Gild J, et al. A new class of high-entropy perovskite oxides. *Scr Mater.* 2018;142:116–120.
- [23] Sarkar A, Djenadic R, Wang D, et al. Rare earth and transition metal based entropy stabilised perovskite type oxides. *J Eur Ceram Soc.* 2018;38:2318–2327.
- [24] Lei Z, Liu X, Li R, et al. Ultrastable metal oxide nanotube arrays achieved by entropy-stabilization engineering. *Scr Mater.* 2018;146:340–343.
- [25] Kotsonis GN, Rost CM, Harris DT, et al. Epitaxial entropy-stabilized oxides: growth of chemically diverse phases via kinetic bombardment. *MRS Commun.* 2018;8:1–7.
- [26] Sharma Y, Musico BL, Gao X, et al. Single-crystal high entropy perovskite oxide epitaxial films. *Phys Rev Mater.* 2018;2:60404.
- [27] Sarkar A, Djenadic R, Usharani NJ, et al. Nanocrystalline multicomponent entropy stabilised transition metal oxides. *J Eur Ceram Soc.* 2017;37:747–754.
- [28] Biesuz M, Spiridigliozzi L, Dell'Agli G, et al. Synthesis and sintering of (Mg, Co, Ni, Cu, Zn)O entropy-stabilized oxides obtained by wet chemical methods. *J Mater Sci.* 2018;53:8074–8085.
- [29] Dupuy AD, Wang X, Schoenung JM. Entropic phase transformation in nanocrystalline high entropy oxides Entropic phase transformation in nanocrystalline high entropy oxides. *Mater Res Lett.* 2019;7:60–67.
- [30] Rahaman MN. *Ceramic processing and sintering.* New York (USA): Marcel Dekker; 1996.
- [31] German RM. *Liquid phase sintering.* New York (USA): Springer Science; 1985.